Performance of a high-sensitivity dedicated cardiac SPECT scanner for striatal uptake quantification in the brain based on analysis of projection data

Mi-Ae Park[a] and Stephen C. Moore
Department of Radiology, Brigham and Women's Hospital and Harvard Medical School, Boston, Massachusetts 02115

Stefan P. Müller
Abteilung Nuklearmedizin, Universitätsklinikum Essen, 45147 Essen, Germany

Sarah J. McQuaid and Marie Foley Kijewski
Department of Radiology, Brigham and Women's Hospital and Harvard Medical School, Boston, Massachusetts 02115

(Received 14 August 2012; revised 20 February 2013; accepted for publication 21 February 2013; published 18 March 2013)

Purpose: The authors have previously reported the advantages of high-sensitivity single-photon emission computed tomography (SPECT) systems for imaging structures located deep inside the brain. DaTscan (Isoflupane I-123) is a dopamine transporter (DaT) imaging agent that has shown potential for early detection of Parkinson disease (PD), as well as for monitoring progression of the disease. Realizing the full potential of DaTscan requires efficient estimation of striatal uptake from SPECT images. They have evaluated two SPECT systems, a conventional dual-head gamma camera with low-energy high-resolution collimators (conventional) and a dedicated high-sensitivity multidetector cardiac imaging system (dedicated) for imaging tasks related to PD.
Methods: Cramer–Rao bounds (CRB) on precision of estimates of striatal and background activity concentrations were calculated from high-count, separate acquisitions of the compartments (right striata, left striata, background) of a striatal phantom. CRB on striatal and background activity concentration were calculated from essentially noise-free projection datasets, synthesized by scaling and summing the compartment projection datasets, for a range of total detected counts. They also calculated variances of estimates of specific-to-nonspecific binding ratios (BR) and asymmetry indices from these values using propagation of error analysis, as well as the precision of measuring changes in BR on the order of the average annual decline in early PD.
Results: Under typical clinical conditions, the conventional camera detected 2 M counts while the dedicated camera detected 12 M counts. Assuming a normal BR of 5, the standard deviation of BR estimates was 0.042 and 0.021 for the conventional and dedicated system, respectively. For an 8% decrease to BR = 4.6, the signal-to-noise ratio were 6.8 (conventional) and 13.3 (dedicated); for a 5% decrease, they were 4.2 (conventional) and 8.3 (dedicated).
Conclusions: This implies that PD can be detected earlier with the dedicated system than with the conventional system; therefore, earlier identification of PD progression should be possible with the high-sensitivity dedicated SPECT camera. © *2013 American Association of Physicists in Medicine*. [http://dx.doi.org/10.1118/1.4794488]

Key words: quantitative SPECT, collimation, phantom study, Cramer-Rao bound, striatal imaging

I. INTRODUCTION

Single-photon emission computed tomography (SPECT) and positron emission tomography (PET) brain imaging have become important tools for Parkinson disease (PD) clinicians and researchers in their efforts to identify disease state, rate of disease progression, and translational biomarkers,[1] as well as for monitoring effects of therapy.[2] SPECT is more widely available than is PET; however, at present, PET provides better spatial resolution and much higher sensitivity. Improved SPECT sensitivity, particularly for imaging central brain structures, would lead to improved reproducibility of SPECT-derived measures, thereby addressing a major current limitation of SPECT imaging for PD.[3] Moreover, increased SPECT sensitivity would mean that fewer subjects would be needed for clinical trials of therapeutic agents.

Several SPECT agents which bind to dopamine transporter (DaT) sites have been developed, including the ^{123}I agents, beta-CIT,[4] and altropane[5] as well as a ^{99m}Tc agent, TRODAT.[6] Two ^{123}I dopamine receptor agents, IBZM (Ref. 7) and IBF,[8] have also been developed, as well as a ^{123}I serotonin transporter tracer.[9] Quantitative estimates of striatal activity concentration, volumes, and kinetic parameters are of clinical significance in several neurological diseases. Reductions in the size and activity concentration of striata, as well as alterations in tracer kinetics, have been reported in

Parkinson disease,[10,11] and abnormalities of the dopaminergic system have also been reported in other movement disorders, including Huntington's disease.[12] One of the most promising agents for PD is N-o-fluoropropyl-2,f-carbomethoxy-3,B (4-iodophenyl)tropane (^{123}I-FP-CIT), used to visualize the DaT using SPECT. Booij *et al.*[11] showed that the uptake of FP-CIT in both the caudate nucleus and putamen of patients with Parkinson's disease was significantly lower than in age-matched controls and, furthermore, that FP-CIT can discriminate patients with early PD from normal controls.

Most clinical SPECT scanners are equipped with parallel-hole collimators, which yield uniform sensitivity across the detector. This is suboptimal because, due to attenuation, relatively fewer photons originating in the deep brain structures that are of greatest interest for PD are detected. This degrades both accuracy and precision of quantitative SPECT studies; while the bias can be addressed by attenuation correction procedures, such techniques do not improve precision. We have previously shown that brain SPECT can benefit from nonuniform transaxial sampling of the projections, with central regions more heavily represented, in order to compensate for loss of information from central brain structures by attenuation.[13] One way to achieve such sampling is to design a collimator that accepts more photons from the central region than from the periphery of the brain[14] or to build a dedicated brain SPECT system, e.g., CeraSPECT.[15] Another approach, which may also improve the sensitivity and/or resolution of the images, is to use a dedicated cardiac scanner. The D-SPECT (Spectrum Dynamics, Caesarea, Israel) is a novel imaging instrument that yields for cardiac applications increased sensitivity, by a factor of up to 10, compared to conventional SPECT instruments.[16]

We have evaluated the D-SPECT for striatal activity estimation and compared it to a conventional dual-head SPECT camera, Symbia T6 (Siemens Medical Solutions, Inc., Knoxville, TN). All calculations were performed on the projection data. The advantage of assessing camera performance based on projection data is that the assessment is independent of the reconstruction algorithm and parameters and, thus, depends solely on the information conveyed by the collimated and detected photons.

II. METHODS

II.A. SPECT scanners

The Siemens Symbia T6 SPECT/CT scanner (Siemens Medical Solutions, Inc., Knoxville, TN) (conventional system) consists of two large rectangular detectors, each with a 53 × 39 cm field of view. The 9.5 mm NaI (Tl) crystals yield better than 10% energy resolution for the 140-keV Tc-99 m photopeak and 3.8 mm intrinsic spatial resolution. For our experiments, the Symbia was equipped with low-energy, high-resolution parallel hole (LEHR) collimators. The hexagonal hole diameter was 1.1 mm (flat-to-flat distance) and the hole length was 24 mm. Each projection dataset consisted of 120 angular views over a 360° circular orbit in a 180° detector configuration with acquisition time 5 s/view. The radius of rotation was 13 cm.

The D-SPECT (Spectrum Dynamics, Caesarea, Israel) (dedicated system) is equipped with 9 cadmium zinc telluride (CZT) solid-state detectors, each consisting of a 16 (transaxial) × 64 (axial) array and capable of individual rotation around its (axial) axis, which corresponds to the vertical direction in Fig. 1(b). Each detector can rotate a maximum of 100°. The detectors can also shift in unison by a half of the detector spacing around an arc in the transaxial plane to measure additional angular projections at positions in between the initial detector positions. This makes it possible to use a flexible acquisition pattern by which photons are detected mainly from a preselected region—in normal clinical use, the heart—to maximize the counts from the organ of interest.[16,17] For each acquisition, the angular scanning pattern is determined for each detector based on a preselected region of interest (ROI). The CZT detectors are characterized by better energy resolution, <6.2% at 140 keV, than are conventional NaI-based detectors. Because of the wide (2.26 mm) tungsten collimator holes, the system is characterized by higher sensitivity compared to a conventional system. The short (21.7 mm) hole length also increases the solid angle for photon acceptance, thereby further increasing sensitivity at the cost of degraded resolution. Gambhir *et al.*[17] showed that it would take ten times longer for a conventional dual-head SPECT camera with LEHR collimation to acquire the same number of detected counts (14.3×10^6) as with D-SPECT,

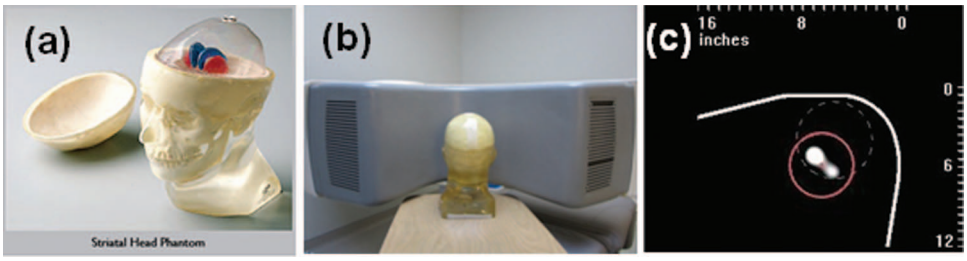

FIG. 1. (a) Magnified view of the striatal phantom with fillable striata (http://www.rsdphantoms.com/nm_striatal.htm). The volume of each compartment is 4.8 ml (right caudate), 4.9 ml (left caudate), 5.8 ml (right putamen), 6.0 ml (left putamen,) and 1260 ml (background). (b) The phantom was positioned on the D-SPECT facing the center of the detector array. (c) A prescan of the phantom on the D-SPECT. The prescan was acquired using a motor file designed for a cardiac imaging. A scan pattern using the motor file focused on the dashed circle that was presumed to enclose the heart. A new circular ROI of 6 cm radius (solid line) was drawn to assign a new scan pattern to maximize the counts from the region. In order to obtain the clearest possible view of the striata, the right and left putamen were filled with Tc-99m while other compartments contained only air.

TABLE I. Specifications and scan parameters for the conventional and dedicated systems.

	Conventional SPECT	Dedicated high-sensitivity SPECT
System	Siemens Symbia T6 SPECT/CT	Spectrum Dynamics D-SPECT
Crystal	NaI (Tl)	Pixelated CZT
# Heads	2	9
Collimator	Hexagonal LEHR (lead)	Parallel square holes (tungsten)
Hole size (mm)	1.11	2.26
Hole length (mm)	24.05	21.7
Detector size (cm/head)	53 × 38	4 × 16
Scan views (views/head)	120	120
Configuration	180 deg	Predefined, flexible scan pattern
Scan duration (s/view)	5	5
Zoom	2.29	1

using a single Co-57 line source, i.e., 45.5 min for conventional vs 4 min for dedicated system. A shorter scan time with the same image quality would provide great benefits for imaging PD patients, some of whom cannot remain still for an extended period. For our phantom experiments, we acquired 120 angular projections from each of the 9 detectors, with a 5 s acquisition time for each. Therefore, to acquire a complete projection dataset required the same time, 10 min, on both systems. In Table I, we summarize the hardware and technical parameters for each system evaluated.

II.B. Phantom experiments

Projection datasets were acquired using the RSD striatal phantom (Radiology Support Devices, Long Beach, CA), consisting of separately fillable compartments for left and right striata and brain background (Fig. 1). (Although the left and right caudate and putamen compartments are separately fillable, we treated each side as a single structure.) We filled one compartment (right or left striata or background) at a time with radioactive Tc-99 m, while the other two compartments were filled with nonradioactive water. Initial activity concentrations were 40–50 μCi/cc for the striatal compartments and 4–5 μCi/cc for the background compartment. After filling each compartment, the phantom was always repositioned in the same location. For acquisitions on the conventional system, the phantom was placed on a headholder and the built-in laser lines were used to reproduce the position for each compartment. Scanning on the D-SPECT required predetermination of the detector scanning pattern. From a quick scan using a standard motor file (which controls the motion of each of the nine detectors), an initial image of the phantom activity was obtained [Fig. 1(c)], on which we drew a circular region which enclosed both the right and the left putamen. The D-SPECT software then generated a new optimized motor file which enabled the system to collect more photons from the striatal region and fewer from less important surrounding regions. For the brain phantom, each detector block swept over 40°–60° from its base position. When the detectors were focusing on the striatal region inside the ROI, the angular increment was 0.6° (fine sampling region). However, when they were collecting data from surrounding regions, the angular increment varied from 0.8° to 2.6° (coarse sampling region). The acquisition time at each angular position was the same for all of the detectors. The scan pattern is illustrated in Fig. 2. The discontinuity at the 60th angular view is due to the detector shift. The same motor file was then used for scanning all compartments. We repositioned the phantom using five-point registration between the detector cover and the phantom, which faced the detector surface [Fig. 1(b)].

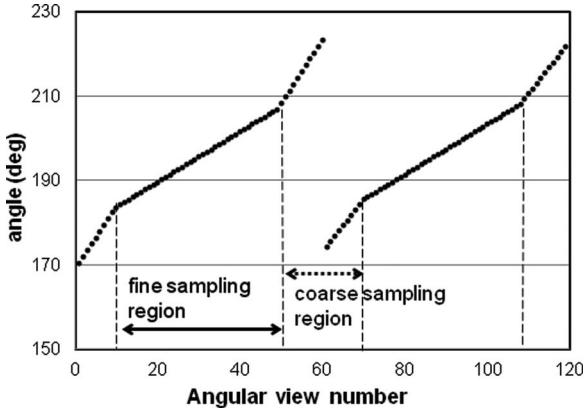

FIG. 2. An example of scan pattern. The angular increment was 0.6° when the detector was collecting data from the fine sampling region. In the coarse sampling region, it varied from 0.8° to 2.6°.

In order to generate very low-noise projection datasets, we used activity concentration values in each compartment that were greater than the expected values; these were low enough to keep the dead-time effect minimal, i.e., below 2%. Furthermore, we obtained multiple (7–10) acquisitions for each compartment; these were summed and normalized to unit activity concentration. Realistic human brain projection datasets were then synthesized by appropriately scaling and summing these essentially noise-free normalized compartment data.

II.C. Estimation of activity concentrations

Typically, a DaTscan acquisition contains 1–2 M total counts over the entire projection dataset. We first scaled our projection data and obtained the activity distribution to achieve 2×10^6 total counts on the conventional system. The same activity distribution was then used to scale and sum compartment projections for both systems. From these data, we calculated the Cramer–Rao bounds (CRB) on the precision of estimates of striatal and background activity concentration. The CRB represented the best possible performance for an unbiased estimator. This approach implicitly incorporates the effects of scatter and attenuation, as well as spatial resolution and sensitivity. Our calculations were based on the

following model:

$$I(\theta, x, y) = S_R f(\theta, x, y) + S_L g(\theta, x, y) + Bh(\theta, x, y), \tag{1}$$

where $f(\theta, x, y)$ and $g(\theta, x, y)$ are the projections of the right and left striata at the pixel position (x, y) on each detector and at the angular view θ. $h(\theta, x, y)$ is the projection of the background, which includes the rest of the brain. S_R and S_L are the activity concentration in the right and left striata, and B is the activity concentration in the background which we assumed to be uniformly distributed. Then a 3×3 Fisher's information matrix, $\mathbf{J}$, was calculated from the projections by

$$J_{ij} = \sum_{\det} \sum_{\theta,x,y} \left[\frac{\partial I(\theta, x, y)}{\partial A_i}\right]\left[\frac{\partial I(\theta, x, y)}{\partial A_j}\right] \cdot \frac{1}{I(\theta, x, y)}, \tag{2}$$

where A_i is the activity concentration in compartment i, i.e., S_R, S_L, or B for our study. There were two detectors for the conventional dual-head system and nine detectors for the dedicated system.

J_{11}^{-1} and J_{22}^{-1} are the CRB on the variance of activity-concentration estimates in the right and left striata, respectively. Therefore, we define a task-specific ideal-estimation signal-to-noise ratio (SNR) for measuring striatal activity

$$\mathrm{SNR}_{\mathrm{right}} = \frac{S_R}{\sqrt{J_{11}^{-1}}},$$
$$\mathrm{SNR}_{\mathrm{left}} = \frac{S_L}{\sqrt{J_{22}^{-1}}}. \tag{3}$$

Note that this quantity is the inverse of the coefficient of variation. We also calculated the SNR for estimating the specific-to-nonspecific binding ratio (BR) using volumes of interest (VOI) in the striata and the occipital cortex, where BR is defined as

$$\mathrm{BR} = \frac{\mathrm{VOI(striata)} - \mathrm{VOI(background)}}{\mathrm{VOI(background)}}, \tag{4}$$

where VOI(striata) is either the right or the left striata.

The CRB on variances of BR estimation were calculated using propagation of error analysis; from these we calculated ideal-estimation SNR for the right and left BR. All calculations used the final projection data, $I(\theta, x, y)$; therefore, pixels in the detectors contained projections from one or more compartments. The variance of BR was affected by variance of each striatum and background, and also by covariance between striatum and background.

To assess the capability of each system to follow disease progression or response to therapy, we also evaluated how precisely they could measure small changes in BR. The ideal-estimation SNR for measuring changes in BR was determined for each system using the following equation:

$$\mathrm{SNR(changes)} = \frac{|\mathrm{BR_{pre}} - \mathrm{BR_{post}}|}{\sqrt{\mathrm{var(BR_{pre})} + \mathrm{var(BR_{post})}}}. \tag{5}$$

$\mathrm{BR_{pre}}$ could be measured from a baseline or previous study, and $\mathrm{BR_{post}}$ may be from a post-treatment measurement or from a follow-up study at a later time point. We estimated the SNR for detecting 5% and 8% decreases in the true value of BR, based on reports that 5%–8% is the range of annual change in BR in early PD.[18,19]

A left-right asymmetry index was shown to be higher in PD compared with healthy controls.[13] It has been also shown that there were differences in the posterior putamen asymmetry indices of PD and dementia with Lewy bodies.[20] The CRB on the precision of estimating the asymmetry index was also calculated from the projection dataset using propagation of errors, and the following equation:

$$\text{Asymmetry index}(\%) = \frac{|\mathrm{BR(high)} - \mathrm{BR(low)}|}{[\mathrm{BR(high)} + \mathrm{BR(low)}]/2} \times 100, \tag{6}$$

where BR(high) and BR(low) are the binding ratio measurements for the higher uptake side and the lower uptake side, respectively.

III. RESULTS AND DISCUSSION

In Fig. 3, we show one projection view for each scanner for each of the three compartments. For the D-SPECT dedicated scanner, all nine detectors are shown, while one detector is presented for the conventional SPECT system. The white pixels in the projections on the dedicated system are disabled crystals; these do not significantly degrade the performance of the system and, of course, they did not contribute to the CRB calculations (zero-valued detector elements are not included). We summed the projections from all angular views and for all three compartments, and compared the total counts. We first fixed the specific-to-nonspecific ratio in terms of BR and then obtained the activity concentration for each region. While the conventional system acquired 2 M counts for a phantom configuration of BR = 5, the dedicated system recorded 12 M for the same phantom configuration, higher than the conventional system by a factor of 6. Gambhir[17] reported gains of 11 for a line source and 7–8 for the cardiac region in patient studies for the D-SPECT compared to a conventional camera; it is not surprising that our gain was lower for a more extended source.

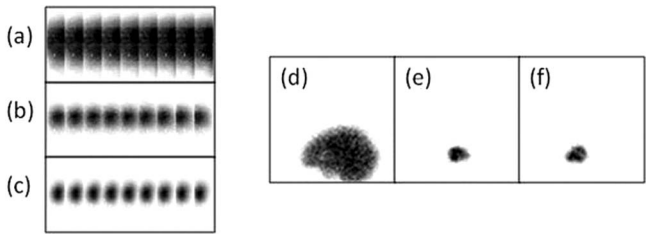

FIG. 3. Projections on the nine D-SPECT detector blocks acquired for 5 s for (a) background filled with 4.2 μCi/cc, (b) left striata filled with 22.6 μCi/cc, and (c) right striata filled with 30.2 μCi/cc. (White dots indicate the locations of disabled crystals.) One 5-s projection view on the Symbia (d) background filled with 4 μCi/cc, (e) left striata filled with 30 μCi/cc, and (f) right striata filled with 44 μCi/cc.

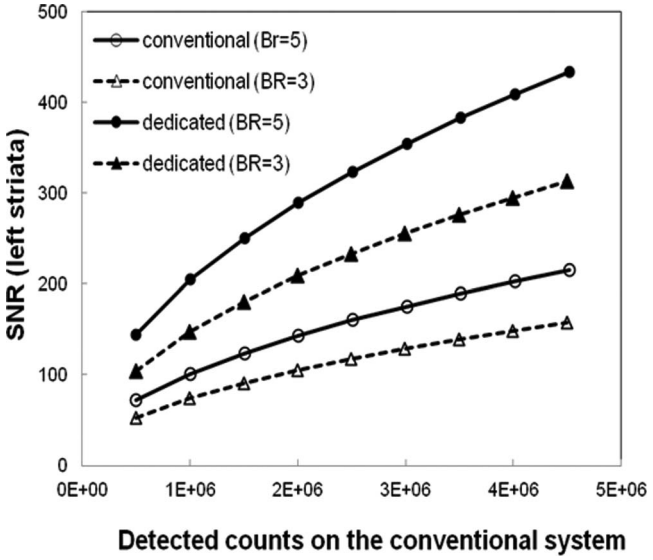

FIG. 4. SNR for estimation of activity concentration in the right striata as a function of total counts detected on the conventional system, for two values of BR.

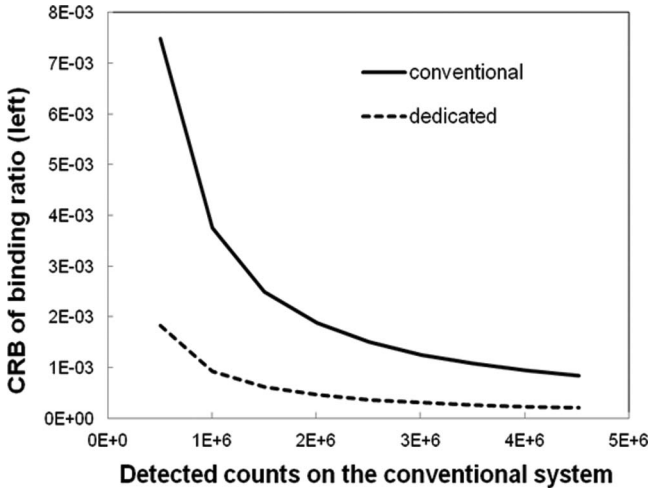

FIG. 5. The CRB on precision of estimates of specific-to-nonspecific BR as a function of total counts detected on the conventional system for BR = 5.

Using Eqs. (3), we calculated the SNR for both systems. For a given number of total counts on the conventional SPECT system, we obtained the activity concentration of the background and striata with a fixed BR, 5 or 3. The same activity concentration distribution was used to simulate the phantom on the dedicated system. Figure 4 shows the ideal-estimation SNR for activity concentration in the left striata. The SNR increases as predicted by the increase in the detected counts for both systems. For BR = 5 and 2 M detected counts on the conventional system, the SNR was 143 for the conventional, and 289 for the dedicated systems. These values decreased to 104 and 208, respectively, for BR = 3. The SNR from the dedicated system was ~2.0 times greater than that from the conventional system. Note that the improvements in task-specific SNR are less than would be expected based on the gains in sensitivity alone. This reflects the task performance penalty due to the D-SPECT's poorer spatial resolution, as well as a suboptimal scanning pattern. An optimal scanning pattern for the brain would require a change in the positions of the detectors.[21] Gambhir[17] reported both improved sensitivity and improved resolution for the D-SPECT compared to a conventional system, based on reconstructed cardiac images. The utility of our approach is that, because it is based on raw acquired data, it reflects the fundamental properties of the instruments without confounding the analysis by the properties of the reconstruction algorithm. Gambhir's[17] image-based comparisons used D-SPECT images reconstructed with resolution recovery and a strong prior and conventional system images reconstructed with neither advantage.

We also calculated the CRB on estimation of the BR by propagation of error analysis based on Eq. (4). The CRB for the dedicated system was 75% lower than that of the conventional system, for an activity concentration distribution yielding 2 M total counts on the dedicated system and BR = 5 (Fig. 5). Overall, for all count level and BR combinations tested, BR could be estimated more precisely with the dedicated system than with the conventional system.

System comparisons on the basis of absolute measurements of striatal uptake or BR for the purposes of identifying between-group differences or classifying individual patients are subject to variability among patients at the same stage of disease, however defined. This may diminish advantages of one scanner over another; however, this is not true of imaging tasks involving serial images of the same patient for, e.g., following disease progression or assessing response to therapy. Scanner comparisons for longitudinal tasks will be affected only by variability resulting from changes over time in patient tracer uptake and technical factors such as repositioning error; these are expected to be minimal compared to interpatient variability.

The SNR values represent the best possible performance of the two systems, assuming an unbiased, efficient estimation procedure (including, implicitly, an unbiased, efficient reconstruction algorithm). Because they are based on phantom experiments, they overstate the performance that would be expected in the clinic. Nonhardware-dependent sources of variability in estimates of striatal uptake or BR would be the same for either system, tending to diminish between-scanner differences. If the estimates are to be used to quantify between-group (e.g., normal vs early PD) differences, or to classify individual patients, then normal interpatient variation should be incorporated into the system comparison.

Winogrodzka *et al.*[18,19] reported an average decline in BR of 8% per year in early PD, with a minimum decline of 5% using both FP-CIT and beta-CIT. The ideal-estimation SNR for detecting these small changes in BR were calculated and summarized in Table II. We assumed that the baseline BR was 5.0 and simulated the post-SPECT imaging for BR = 4.75 and 4.6 for 5% and 8% decrease, respectively. The results showed that the dedicated system can measure these small changes more precisely, improving the SNR by a factor of 1.96.

The smallest detectable decrease in BR for both systems was calculated. We determined the activity concentration in the phantom that yielded for 2 M detected counts on the

TABLE II. The signal-to-noise ratio for detecting a small change in binding ratio with the baseline BR = 5.0.

Total counts on the conventional system	5% decrease		8% decrease	
	Conventional	Dedicated	Conventional	Dedicated
1.0×10^6	2.99	5.86	4.81	9.41
2.0×10^6	4.23	8.30	6.80	13.30
3.0×10^6	5.19	10.16	8.32	16.29

conventional system with BR = 5, and applied the same concentration to both systems. The BR was then decreased by a small amount and SNR for detecting the decrease was calculated using Eq. (4). The minimum decrease in BR which can be detected with SNR = 4 was 4.8% for the conventional and 2.6% for the dedicated system.

The amount of dopamine transporter tends to become asymmetric depending on the progress of the disease. We have calculated an asymmetry index which mimics such a clinical case by making the uptake in one side of the striata lower than the opposite side. In our phantom, we made the left striata 10%–30% lower than the right striata. When the value of BR in the left striata decreased by 10%, 5% for the right, and 4.5% for the left striata, the asymmetry index becomes 10.5% from Eq. (5). For the 20% decrease, the asymmetry index was 22.2%. Using Eq. (5) and propagation of error analysis, we calculated the variance and the SNR on the estimation of the asymmetry index. Using the activity level in the phantom to achieve 2 M detected counts on the conventional system, the SNR was plotted in Fig. 6 as a function of the asymmetry index for BR = 5 and 4. The SNR increased as the asymmetry index increased. For the same BR, the dedicated system offered higher SNR compared to the conventional system. The precise measurement of small changes of BR in the early stages of the disease—or following therapeutic intervention—should be very useful for investigating disease progression and for evaluation of the effect of treatments. With the gain in sensitivity and precision, fewer subjects may be needed for clinical trials of therapeutic agents.

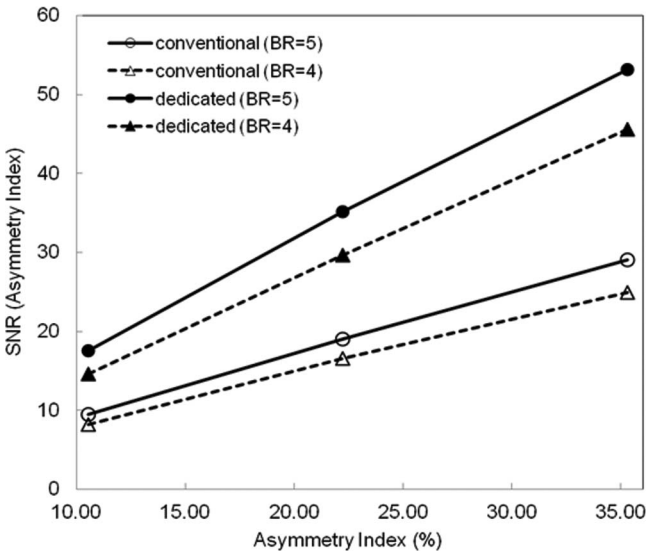

FIG. 6. SNR for measuring asymmetry index, as a function of asymmetry ratio, for two values of BR.

These results demonstrate the potential of a design similar to the D-SPECT, but optimized for brain imaging; such a system would, presumably, yield even better performance in tasks such as the ones we analyzed. The current D-SPECT hardware configuration is suboptimal for brain imaging because of the limited angular coverage [see Fig. 1(b)]. The D-SPECT configuration was designed for cardiac imaging; it is likely that a scanner optimized for brain imaging would more fully surround the brain. A reconfigured system that retains the scanning detectors, such as the one proposed by Erlandsson *et al.*[21] could provide data acquisition that adapts to various brain imaging tasks, and focuses on volumes of interest.

For the same scan time, the dedicated system showed better performance, yielding lower variance and, consequently, higher task-specific SNR, for all the quantities we simulated. Likewise, patients who cannot lie still for the scan time required to detect expected changes on a conventional system can be imaged in a shorter time using the dedicated system. Implicit in the calculation of our CRB-based metrics are several assumptions. It is assumed that the estimators incorporate accurate information on the size, shape, and location of the anatomic structures and, furthermore, accurate information on the system model, including scatter and attenuation. Furthermore, the CRB represents the best possible precision of an unbiased estimator; it is sometimes possible to achieve lower variance with a biased estimator. Also, because we used Tc-99 m instead of I-123 for the phantom acquisitions, our data included fewer photons that had penetrated the collimator septa than would be true of a DaTscan acquisition. We expect that, had we used I-123, the D-SPECT would be less affected by septal penetration because of its relatively thick septa (0.2 mm compared to 0.16 mm for the conventional system).[16] Because we based our comparison on raw acquired projection data, our comparison is based on fundamental hardware properties, and not affected by characteristics of image reconstruction and correction algorithms. The performance improvement for the dedicated system is large enough that effects due to software would not be expected to alter the results very much.

The CRB represents the best possible performance (minimum variance) of an unbiased estimator. If the projections are reconstructed by filtered backprojection, which under certain conditions is unbiased and efficient,[22] then we would expect that an unbiased, efficient estimator of a quantitative metric using these images would match the performance of the CRB calculated from the projections. Iterative algorithms differ from analytical algorithms in that they offer an explicit trade-off between resolution recovery and level of noise, i.e., there is the option to choose a biased reconstruction with reduced noise. Estimation in this case can lead to better reproducibility (lower variance) performance than predicted from the CRB at the cost of degraded accuracy. Reconstruction algorithms which utilize *a priori* information would, of course, be expected to yield better estimation performance than predicted by the CRB, unless the CRB model were adjusted to

incorporate the *a priori* information. In this case, however, we would be confounding effects that are solely attributable to the fundamental performance of the imaging systems with those of the prior, which is usually just based on properties of the object being imaged, rather than on the imaging system. For these reasons, we believe that calculating CRB from the projection datasets is a more meaningful approach to assessing performance in quantitative tasks than is calculating CRB from reconstructed images. Furthermore, the reconstruction algorithm is not a fundamental property of SPECT systems, as it is relatively easy to change. Finally, it is important to note that CRB calculated from the projections can serve as standards of optimal task performance even for quantities which, in clinical practice, would usually be calculated from reconstructed images.

It is important to note that the imaging tasks considered here are estimation of striatal activity concentration, with striatal boundaries known exactly, in the presence of a background of unknown activity, and estimation of quantities derived from striatal or background activity estimates. We have shown previously that tasks which, like these, are linear in the data, are less demanding in terms of spatial resolution than are more complex tasks, such as estimation of activity within a structure whose boundaries are unknown.[23] Therefore, it is not surprising that we found that the task-dependent SNR were much higher for a system with very high sensitivity (dedicated) than for a system with lower sensitivity but better spatial resolution (conventional). For these tasks, the performance of the conventional system could be improved by using a collimator with increased sensitivity, even with some loss of resolution. Furthermore, the sensitivity of the conventional system could be improved without loss of resolution by using a collimator with centrally peaked sensitivity.[13,14] However, the advantage of the D-SPECT design is flexibility. Unlike the conventional system, the D-SPECT can be easily configured for optimal scanning of arbitrary regions of interest. For SPECT/CT systems such as the conventional one, boundaries of some structures can be obtained from the registered CT image, although anatomical boundaries of a structure may not match the functional boundaries of the radioactivity uptake. Striata are not well visualized on CT and, in any case, structural and functional boundaries are not likely to match in disease.[24] For tasks which require estimation of structure (functional) boundaries, as well as structure activity concentration, from the SPECT image, we would expect that the advantages of the dedicated system over the conventional system would be reduced.

We have calculated the performance of the two systems based on projections rather than from reconstructed images. The advantage of this approach is that the results are independent of the choice of reconstruction algorithm. We have shown previously that the SNR values from projection data are very close to those calculated from images reconstructed using filtered backprojection.[23] Since diagnoses in brain imaging are commonly made on the reconstructed 3D brain images, it would be useful if the dedicated system could generate 3D volume images of the brain. The D-SPECT system is widely used for cardiac imaging and a 3D volume of the heart is reconstructed from projections. The reconstruction may involve better understanding of the location of the object being imaged, i.e., the striata in our study, relative to the detectors and the rotational views of each detector. From our experience with phantom imaging throughout the current study, we believe that the reconstruction of the striata is not much different than the reconstruction of the heart. A dedicated SPECT system is expensive and not available in many sites. Our study showed that a scanner dedicated for imaging one organ could be used for imaging other organs, assuming that it provides clinically valuable images. Although the dedicated system we used was developed specifically for cardiac imaging, our results imply that it could be very worthwhile for the manufacturer to develop a similar dedicated brain scanner along with a reconstruction algorithm tailored for brain imaging.

IV. CONCLUSIONS

We have demonstrated the potential of a dedicated cardiac SPECT system for quantitative assessment of centrally located brain regions, such as the striata. The results of our analyses implied that the increased sensitivity of the D-SPECT over the conventional system leads to significantly improved performance in estimating clinically important metrics, such as striatal uptake, binding ratio, and the left-right asymmetry index, even though the system was not optimized for these tasks. We believe that the flexible, scanning-detector design of the D-SPECT has great potential for brain imaging.

ACKNOWLEDGMENT

This work was supported in part by the NIH under Grant Nos. R01-EB000802 and R01-EB001989.

[a]Author to whom correspondence should be addressed. Electronic mail: miaepark@bwh.harvard.edu.

[1]D. J. Brooks, "Imaging approaches to Parkinson disease," J. Nucl. Med. **51**, 596–609 (2010).
[2]J. Booij and H. W. Berendse, "Monitoring therapeutic effects in Parkinson's disease by serial imaging of the nigrostriatal dopaminergic pathway," J. Neurol. Sci. **310**, 40–43 (2011).
[3]P. K. Morrish, "The harsh realities facing the use of SPECT imaging in monitoring disease progression in Parkinson's disease," J. Neurol., Neurosurg. Psychiatry **74**, 1447 (2003).
[4]R. B. Innis *et al.*, "Single photon emission computer tomographic imaging demonstrates loss of striatal dopamine transporters in Parkinson disease," Proc. Natl. Acad. Sci. U.S.A. **90**, 11965–11969 (1993).
[5]A. J. Fischman *et al.*, "Rapid detection of Parkinson's disease by SPECT with altropane: A selective ligand for dopamine transporters," Synapse **29**, 128–241 (1998).
[6]H. F. Kung, H. Kim, M. Kung, S. Meegalia, K. Plossl, and H. Lee, "Imaging of dopamine transporters in humans with technetium-99m TRODAT-1," Eur. J. Nucl. Med. **23**, 1527–1530 (1996).
[7]J. Schwarz, K. Tatsch, G. Arnold, T. Gasser, C. Trenwalder, C. M. Kirsch, and W. H. Oertel, "123I-iodobenzamide-SPECT predicts dopaminergic responsiveness in patients with de novo parkinsonism," Neurology **42**, 556–561 (1992).
[8]M. Kung, H. Kung, J. Billings, Y. Yang, R. A. Murphy, and A. Alavi, "The characterization of IBF as a new selective dopamine D-2 receptor imaging agent," J. Nucl. Med. **31**, 648–654 (1990).

[9]T. A. Kauppinen, K. A. Bergstrom, P. Heikman, J. Hiltunen, and A. K. Ahonen, "Biodistribution and radiation dosimetry of [^{123}I]ADAM in healthy human subjects: Preliminary results," Eur. J. Nucl. Med. **30**, 132–136 (2003).
[10]S. Asenbaum, T. Brucke, W. Pirker, I. Podreka, P. Angelberger, S. Wenger, C. Wober, C. Muller, and L. Deecke, "Imaging of dopamine transporters with iodine-123-beta-CIT and SPECT in Parkinson's disease," J. Nucl. Med. **38**, 1–6 (1997).
[11]J. Booij, G. Tissingh, G. J. Boer, J. D. Speelman, J. C. Stoof, A. G. M. Janssen, E. C. Wolters, and E. A. van Royen, "I-123 FP-CIT SPECT shows a pronounced decline of striatal dopamine transporter labeling in early and advanced Parkinson's disease," J. Neurol., Neurosurg. Psychiatry **62**, 133–140 (1997).
[12]M. Ichise, H. Toyama, L. Fornazzari, J. R. Ballinger, and J. C. Kirsh, "Iodine-123-IBZM Dopamine-D2 receptor and Technetium-99m-HMPAO brain perfusion SPECT in the evaluation of patients with and subjects at risk for Huntington's-disease," J. Nucl. Med. **34**, 1274–1281 (1993).
[13]M. F. Kijewski, S. P. Muller, and S. C. Moore, "Nonuniform collimator sensitivity: Improved precision for quantitative SPECT," J. Nucl. Med. **38**, 151–156 (1997).
[14]M. Park, S. M. Moore, and M. F. Kijewski, "Brain SPECT with short focal-length cone-beam collimation," Med. Phys. **32**, 2236–2244 (2005).
[15]S. Genna, J. Ouyang, and W. Xia, "Annular single-crystal emission tomography systems," in *The Fundamentals of PET and SPECT*, edited by M. N. Wernick and J. N. Aarsvold (Academic, New York, 2004), pp. 167–178.
[16]K. Erlandsson, K. Kacperski, D. van Gramberg, and B. F. Hutton, "Performance evaluation of D-SPECT: A novel SPECT system for nuclear cardiology," Phys. Med. Biol. **54**, 2635–2649 (2009).
[17]S. S. Gambhir, D. S. Bernan, J. Ziffer, M. Nagler, M. Sandler, J. Patton, B. Hutton, T. Sharir, S. B. Haim, and S. B. Haim, "A novel high-sensitivity rapid-acquisition single-photon cardiac imaging camera," J. Nucl. Med. **50**, 635–643 (2009).
[18]A. Winogrodzka, P. Bergmans, J. Booij, E. A. van Royen, A. G. M. Janssen, and E. Ch. Wolters, "[^{123}I]FP-CIT SPECT is a useful method to monitor the rate of dopaminergic degeneration in early-stage Parkinson's disease," J. Neural Transm. **108**, 1011–1019 (2001).
[19]A. Winogrodzka, P. Bergmans, J. Booij, E. A. van Royen, J. C. Stoof, and E. C. Wolters, "[^{123}I]beta-CIT SPECT is a useful method for monitoring dopaminergic degeneration in early stage Parkinson's disease," J. Neurol., Neurosurg. Psychiatry **74**, 294–298 (2003).
[20]Z. Walker, D. C. Costa, R. W. H. Walker, L. Lee, G. Livingston, E. Jaros, R. Perry, I. McKeith, and C. L. E. Katona, "Striatal dopamine transporter in dementia with Lewy bodies and Parkinson disease," Neurology **62**, 1568–1572 (2004).
[21]K. Erlandsson, E. Howell, N. Roth, and B. F. Hutton, "Assessing possible use of CZT technology for application to brain SPECT," in *Proceedings of the IEEE Nuclear Science Symposium and Medical Imaging Conference*, Valencia (IEEE, Piscataway, NJ, 2011), pp. 3354–3358.
[22]K. A. Hanson, "On the optimality of the filtered backprojection algorithm," J. Comput. Assist. Tomogr. **4**(3), 361–363 (1980).
[23]S. P. Muller, M. F. Kijewski, S. C. Moore, and B. L. Holman, "Maximum-likelihood estimation: A mathematical model for quantitation in nuclear medicine," J. Nucl. Med. **31**, 1693–1701 (1990).
[24]C. Y. Lin, S. H. Liou, C. M. Hsiech, C. K. Huang, and S. Tsai, "Tc-99m TRODAT findings in a mercury-exposed worker," Clin. Nucl. Med. **33**, 719–720 (2008).